*Inorg. Chem.* **2002**, *41*, 6997–7005


# Mass Effect on the Equienergetic High-Spin/Low-Spin States of Spin-Crossover in 4,4′-Bipyridine-Bridged Iron(II) Polymeric Compounds: Synthesis, Structure, and Magnetic, Mössbauer, and Theoretical Studies

**Nicolás Moliner,[1a] M. Carmen Muñoz,[1b] Sylvie Létard,[1a] Lionel Salmon,[1c] Jean-Pierre Tuchagues,[1c] Azzedine Bousseksou,*[,1c] and José Antonio Real*[,1a]**

*Institut de Ciencia Molecular/Departament de Química Inorgànica, Universitat de València, Dr. Moliner 50, 46100 Burjassot, València, Spain, Departament de Física Aplicada, Universitat Politécnica de València, Camino de Vera s/n, 46071, Valencia, Spain, and Laboratoire de Chimie de Coordination du CNRS, UPR 8241, 205 Route de Narbonne, 31077 Toulouse, France*

Received June 4, 2002

The suitability of the system [Fe(4,4′-bipy)$(H_2O)_2(NCX)_2$]·(4,4′-bipy), where 4,4′-bipy stands for 4,4′-bipyridine and X = S (**1**) and Se (**2**), as a precursor for the synthesis of new polymeric spin-crossover compounds has been studied. The reaction of **1** or **2** with bt (2,2′-bithiazoline) afforded the polymeric compounds of formula [Fe(4,4′-bipy)(bt)$(NCX)_2$] (X = S (**3**), Se (**4**)). Compounds **3** and **4** are isostructural, but only the crystal structure of **3** has been fully determined. It crystallizes in the orthorhombic system, *Fdd*2 space group, $Z = 24$, with $a = 38.962(8)$ Å, $b = 11.545(2)$ Å, $c = 30.889(6)$ Å, $V = 13895(5)$ Å$^3$. The structure consists of linear chains constituted by *trans*-4,4′-bipy linked iron(II) ions; two *cis* equatorial positions are occupied by two pseudohalide ligands, and the remaining positions are filled by the bidentate bt ligand. Investigation of their magnetic properties and Mössbauer spectra has revealed the occurrence of a low-spin (LS) ↔ high-spin (HS) conversion involving 12% (**3**, S) and 20% (**4**, Se) of the Fe(II) ions. The thermal variation of the HS fraction is gradual with onset temperatures as low as 60 K. A theoretical approach based on the Ising-like model, completed with molecular vibrations, through harmonic oscillators, fits the data successfully, leading to an energy gap of 65 cm$^{-1}$ (**3**) and 86 cm$^{-1}$ (**4**) between the lowest LS and HS levels, and an average vibration frequency $\bar{\omega}_{LS}$ of 382 cm$^{-1}$ (**3**) and 365 cm$^{-1}$ (**4**) in the LS state. The ca. 1.05 $\omega_{LS(3)}/\omega_{LS(4)}$ ratio is close to the ca. 1.09 Se/S molar mass ratio. The simple electrovibrational Ising-like model permits us to explain, for the first time, a mass effect through the molecular vibrations in a spin-crossover complex that is in the unusual situation of equienergy among the HS and LS states.

## Introduction

The reversible change between low-spin (LS) and high-spin (HS) states induced by temperature or pressure variation or by light irradiation is a well-established phenomenon mainly observed for some pseudo-octahedral iron(II) coordination compounds.[2,3] The spin-crossover involves population/depopulation of the $e_g$ and $t_{2g}$ orbitals as well as concomitant changes in metal-to-ligand bond distance. The average metal-to-ligand bond length is ca. 0.2 Å shorter in the LS state where the $e_g$ orbitals are depopulated. This difference in molecular size and shape between the two spin states plays a central role in the cooperativeness of the phenomenon.[4] Magnetic and optical properties may switch sharply in a very small range of temperature and/or pressure for cooperative transitions. This singularity makes the spin-crossover phenomenon one of the most interesting examples of molecular bistability. Cooperativeness depends on how efficiently the intramolecular changes associated with the spin-conversion are transmitted far into the crystal. An

* To whom correspondence should be addressed. E-mail: jose.a.real@uv.es.

(1) (a) Institut de Ciencia Molecular/Departament de Química Inorgànica, Universitat de València. (b) Departament de Física Aplicada, Universitat Politécnica de Vàlencia. (c) Laboratoire de Chimie de Coordination du CNRS.

(2) Gütlich, P. *Struct. Bonding (Berlin)* **1981**, *44*, 83.

(3) Gütlich, P.; Hauser, A.; Spiering, H. *Angew. Chem., Int. Ed. Engl.* **1994**, *33*, 2024.

(4) König, E. *Prog. Inorg. Chem.* **1987**, *35*, 527.

10.1021/ic0203825 CCC: $22.00 
Published on Web 11/21/2002

interesting approach to explore this efficiency consists of connecting the spin changing centers to suitable bridging ligands.

Self-assembly of molecules driven by coordination to transition metal ions has motivated intense research activity because of their chemical and structural diversity, potential functionality, and beauty.[5] In this context, self-assembly represents an important tool to explore systematically the cooperative effect as the coordination geometry of iron(II) may be propagated into infinite architectures of varying dimensionality and topology. In this respect, rodlike ligands of the polypyridine type have proved to be particularly suitable both for metallo-supramolecular chemistry and the field of spin-crossover materials. However, the examples of polymeric spin-crossover compounds reported up to now are still scarce.[6−11]

Recently, we have reported preliminary results on the synthesis and structural characterization of $[Fe(L^1)(H_2O)_2(NCX)_2]\cdot L^1$ ($L^1$ = 4,4′-bipyridine (4,4′-bipy)) (S(**1**), Se(**2**)) and $[Fe(L^2)(CH_3OH)_2(NCX)_2]\cdot L^2$ ($L^2$ = 4,4′-azopyridine (4,4′-azpy)) and X = S, Se two-dimensional polymers.[12] These structures revealed the formation of *trans*-L-bridged $[Fe(NCX)_2(Y)_2]$ (Y = $H_2O$, $CH_3OH$) linear chains assembled into two-dimensional networks by hydrogen bonds between the uncoordinated ligand L and the coordinated solvent molecules. The coordination sphere is defined by the $[FeN_4O_2]$ chromophore, and consequently, the iron(II) ion is in the HS ground state as expected. This supramolecular pattern has been observed for other M(II)−4,4′-bipy systems (M(II) = Mn, Cu, Zn, Co)[13−16] and $[Mn(bpe)(NCS)_2(H_2O)_2]\cdot$bpe (bpe = 1,2-*trans*-(4-pyridyl)-ethene).[17] Because of their reliability, **1** and **2** may be considered as precursors of new polymeric iron(II) spin-crossover compounds: the water molecules may be substituted for more appropriate nitrogen-donor ligands. As a first step along this line, we have chosen the bidentate 2,2′-bithiazoline (bt) ligand (Chart 1). The present contribution embodies the synthesis, crystal structures, and physical characterization of **1**, **2**, and [Fe(4,4′-bipy)(bt)$(NCX)_2$] (X = S(**3**), Se(**4**)) to illustrate this strategy. On the basis of the thermal variation of the HS molar fraction obtained from the magnetic susceptibility and Mössbauer measurements, performed on compounds **3** and **4**, we report new evidence for a spin-state conversion governed by intramolecular vibrations,[18] as a result of the theoretical analysis carried out with an adequate electrovibrational model.[19]

**Chart 1**

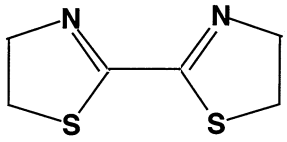


2,2′-bithiazoline (bt)

## Experimental Section

**Materials.** All reagents were of analytical grade and used without further purification. The ligand bt was synthesized according to the method published elsewhere.[20] All complexes were prepared under an argon atmosphere in order to prevent oxidation of iron(II).

**Synthesis of 1 and 2.** A solution of $FeSO_4\cdot 7H_2O$ (0.5 mmol) in methanol (5 mL) was added dropwise to a solution of KNCX (X = S, Se) (1 mmol, 5 mL) in the same solvent. The mixture was stirred at room temperature for 15 min. The $K_2SO_4$ precipitate was filtered off. The colorless 1:2 Fe(II)/$NCX^-$ solution was added dropwise to a solution of 4,4′-bipy (1 mmol) in methanol (20 mL). The red precipitate that formed immediately was isolated by filtration and dried in an argon stream. Crystals suitable for X-ray structure analysis were grown from a 1:1 methanol/water solution of **1** and **2** by slow evaporation (two weeks). Anal. Calcd for $C_{22}H_{20}N_6O_2S_2Fe$ (**1**): C, 50.78; H, 3.85; N, 16.16. Found: C, 50.45; H, 3.76; N, 15.98. Anal. Calcd for $C_{22}H_{20}N_6O_2Se_2Fe$ (**2**): C, 43.01; H, 3.26; N, 13.68. Found: C, 42.60; H, 3.20; N, 13.50.

**Synthesis of 3 and 4.** A solution of bt (0.25 mmol) in methanol/chloroform (1:1, 10 mL) was added dropwise to a solution of **1** (for **3**) or **2** (for **4**) (0.25 mmol) in water/methanol (1:1, 30 mL). The resultant dark-blue solution was stirred for 15 min and then filtered and allowed to concentrate in an argon stream. A very crystalline violet solid was obtained after one week. The solid was filtered off, washed with methanol, and dried. Single crystals of **3** and **4** suitable for X-ray analysis were separated from this solid. Yield 60% (**3**). Anal. Calcd for $C_{18}H_{16}N_6S_4Fe$ (**3**): C, 43.21; H, 3.20; N, 16.80. Found: C, 43.18; H, 3.18; N, 16.76. Yield 40%

(5) Batten, S. R.; Robson, R. *Angew. Chem., Int. Ed.* **1998**, *37*, 1460.
(6) Vreugdenhil, W.; van Diemen, J. H.; De Graaff, R. A. G.; Haasnoot, J. G.; Reedijk, J.; Kahn, O.; Zarembowitch, J. *Polyhedron* **1990**, *9*, 2971.
(7) Ozarowski, A.; Shunzhong, Y.; McGarvey, B. R.; Mislankar, A.; Drake, J. E. *Inorg. Chem.* **1991**, *30*, 3167.
(8) Real, J. A.; Andrés, E.; Muñoz, M. C.; Julve, M.; Granier, T.; Bousseksou, A.; Varret, F. *Science* **1995**, *268*, 265.
(9) Kahn, O.; Martinez, J. C. *Science* **1998**, *279*, 44.
(10) (a) Garcia, Y.; Kahn, O.; Rabardel, L.; Chansou, B.; Salmon, L.; Tuchagues, J. P. *Inorg. Chem.* **1999**, *38*, 4663. (b) Koningsbruggen, P. J.; Garcia, Y.; Kahn, O.; Fournès, L.; Kooijman, H.; Speck, A. L.; Haasnoot, J. G.; Moscovici, J.; Provost, K.; Michalowicz, A.; Renz, F.; Gütlich, P. *Inorg. Chem.* **2000**, *39*, 1981.
(11) Moliner, N.; Muñoz, M. C.; Létard, S.; Solans, X.; Menéndez, N.; Goujon, A.; Varret, F.; Real, J. A. *Inorg. Chem.* **2000**, *39*, 5390. (b) Niel, V.; Martinez-Agudo, J. M.; Muñoz, M. C.; Gaspar, A. B.; Real, J. A. *Inorg. Chem.* **2001**, *40*, 3838.
(12) Moliner, N.; Muñoz, M. C.; Real, J. A. *Inorg. Chem. Commun.* **1999**, *2*, 25.
(13) Li, M.-X.-G.; Xie, G.; Gu, Y.-D.; Chen, J.; Zheng, P.-J. *Polyhedon* **1995**, *9*, 1235.
(14) Chen, X. M.; Tong, M.-L.; Luo, Y.-J.; Chen, Z.-N. *Aust. J. Chem.* **1996**, *49*, 835.
(15) Carlucci, L.; Ciani, G.; Proserpio, D. M.; Sironi, A. *J. Chem. Soc., Dalton Trans.* **1997**, 1801.
(16) Lu, J.; Paliwala, T.; Lim, S. C.; Yu, C.; Niu, T.; Jacobson, A. J. *Inorg. Chem.* **1997**, *36*, 923.
(17) De Munno, G.; Armentano, D.; Poerio, T.; Julve, M.; Real, J. A. *J. Chem. Soc., Dalton Trans.* **1999**, 1813.
(18) (a) Bousseksou, A.; Verelst, M.; Constant-Machado, H.; Lemercier, G.; Tuchagues, J.-P.; Varret, F. *Inorg. Chem.* **1996**, *35*, 110. (b) Bousseksou, A.; Salmon, L.; Varret, F.; Tuchagues, J.-P. *Chem. Phys. Lett.* **1998**, 209−214. (c) Salmon, L.; Donnadieu, B.; Bousseksou, A.; Tuchagues, J. P. *C. R. Acad. Sci.* **1999**, *2*, 305.
(19) (a) Bousseksou, A.; Constant-Machado, H.; Varret, F. *J. Phys. I* **1995**, *5*, 747. (b) Bousseksou, A.; McGarvey, J. J.; Varret, F.; Real, J. A.; Tuchagues, J−P.; Dennis, A. C.; Boillot, M.-L. *Chem. Phys. Lett.* **2000**, *318*, 409. (c) Moliner, N.; Salmon, L.; Capes, L.; Carmen Muñoz, M.; Létard, J.-F.; Bousseksou, A.; Tuchagues, J.-P.; McGarvey, J. J.; Dennis, A. C.; Castro, M.; Burriel, R.; Real, J. A. *J. Phys. Chem. B* **2002**, *106*, 4276. (d) Molnár, G.; Niel, V.; Gaspar, A. B.; Real, J. A.; Zwick, V.; Bousseksou, A.; McGarvey, J. J. *J. Phys. Chem. B* **2002**, *106*, 4276.
(20) Nelson, J.; Nelson, S. M.; Perry, W. D. *J. Chem Soc., Dalton Trans* **1976**, 1282.

**Table 1.** Selected Crystal Data for **3** at 293 K

| | |
|---|---|
| formula | $C_{18}H_{16}N_6S_4Fe$ |
| fw | 500.46 |
| space group | *Fdd*2 |
| *a*, Å | 38.962(8) |
| *b*, Å | 11.545(2) |
| *c*, Å | 30.889(6) |
| *V*, Å$^3$ | 13895(5) |
| *D*(calcd), g cm$^{-3}$ | 1.435 |
| *Z* | 24 |
| $\mu$, cm$^{-1}$ | 10.28 |
| no. indep reflns | 3117 |
| refinement on | $F^2$ |
| R1, wR2[a] | 0.039, 0.101 |
| *S* | 1.06 |
| *T*, K | 293 K |
| $\lambda$ | 0.71073 |

[a] $R1 = \sum||F_o| - |F_c||/\sum|F_o|$; $wR2 = [\sum[w(F_o^2 - F_c^2)^2]/\sum[w(F_o^2)^2]]^{1/2}$. $w = 1/[\sigma^2(F_o^2) + (0.0934P)^2 + 15.3661P]$ where $P = (F_o^2 + 2F_c^2)/3$.

(**4**). Anal. Calcd for $C_{18}H_{16}N_6S_2Se_2Fe$ (**4**): C, 36.37; H, 2.69; N, 14.14. Found: C, 36.04; H, 2.62; N, 13.81.

**Solution and Refinement of the X-ray Structures.** Diffraction data for **3** were collected at 293 K with an Enraf-Nonius CAD4 diffractometer using graphite-monochromated Mo K$\alpha$ radiation ($\lambda$ = 0.71073 Å). The cell parameters were determined from least-squares refinement of 25 well-centered reflections in the range 12° < $\theta$ < 20°. Crystal parameters and refinement data are summarized in Table 1. Three standard reflections were monitored every hour, but no intensity variation was observed. Lorentz-polarization and absorption corrections were applied to the data. The structures were solved by direct methods using SHELXS-86[21] and refined by full-matrix least-squares method on $F^2$ for 395 refined parameters using SHELXL-93.[22] All non-hydrogen atoms were refined anisotropically. The hydrogen atoms were set in calculated positions and refined as riding atoms with a common fixed isotropic thermal parameter. The final full-matrix least-squares refinement on $F^2$, minimizing the function $\sum w[(|F_o|)^2 - (|F_c|)^2]$, converged at the values of R1 and wR2 listed in Table 1. The residual maxima and minima in the final Fourier-difference maps were 0.355 and −0.239. Selected bond lengths and angles are gathered in Table 2.

**Magnetic Measurements.** The variable temperature magnetic susceptibility measurements were carried out on samples (10−15 mg) constituted by small single crystals of **1**−**4** using a Quantum Design MPMS2 SQUID susceptometer equipped with a 55 kG magnet and operating in the ranges 0.1−1 T and 1.8−300 K. The susceptometer was calibrated with $(NH_4)_2Mn(SO_4)_2 \cdot 12H_2O$. Experimental susceptibilities were corrected for diamagnetism of the constituent atoms by using Pascal's constants.

**Mössbauer Spectra.** The variable-temperature Mössbauer measurements were obtained on a constant-acceleration conventional spectrometer with a 50 mCi source of $^{57}$Co (Rh matrix). Isomer shift (IS) values are given with respect to metallic iron at room temperature. The absorber was a sample of about 100 mg of microcrystalline powder of **3** or **4** enclosed in a 20 mm diameter cylindrical plastic sample holder, the size of which had been determined to optimize the absorption. Variable-temperature spectra were obtained in the 305−4.2 K range, by using an MD306 Oxford cryostat, the thermal scanning being monitored by an Oxford ITC4 servocontrol device (±0.1 K accuracy). A least-squares computer program[23] was used to fit the Mössbauer parameters and determine their standard deviations of statistical origin (given in parentheses).

**Table 2.** Selected Bond Lengths (Å)[a] and Angles (deg)[a] for **3**

| | | | |
|---|---|---|---|
| Fe(1)−N(1) | 2.222(10) | Fe(2)−N(9) | 2.06(2) |
| Fe(1)−N(2) | 2.229(13) | S(2)−C(9) | 1.64(2) |
| Fe(1)−N(3) | 2.064(13) | S(5)−C(26) | 1.62(3) |
| Fe(2)−N(4) | 2.256(10) | S(6)−C(27) | 1.63(2) |
| Fe(2)−N(5) | 2.247(10) | N(3)−C(9) | 1.14(2) |
| Fe(2)−N(6) | 2.193(13) | N(8)−C(26) | 1.15(3) |
| Fe(2)−N(7) | 2.220(13) | N(9)−C(27) | 1.12(2) |
| Fe(2)−N(8) | 2.079(14) | | |
| N(1)−Fe(1)−N(1)$^{i}$ [b] | 179.7(8) | N(5)−Fe(2)−N(6) | 88.0(4) |
| N(1)−Fe(1)−N(2) | 93.1(5) | N(5)−Fe(2)−N(7) | 91.1(4) |
| N(1)$^{i}$−Fe(1)−N(2) | 87.1(5) | N(5)−Fe(2)−N(8) | 91.2(5) |
| N(1)−Fe(1)−N(3) | 88.0(5) | N(5)−Fe(2)−N(9) | 89.6(5) |
| N(2)−Fe(1)−N(2)$^{i}$ | 74.3(7) | N(6)−Fe(2)−N(7) | 74.3(5) |
| N(2)−Fe(1)−N(3) | 93.9(5) | N(6)−Fe(2)−N(8) | 90.1(6) |
| N(3)−Fe(1)−N(3)$^{i}$ | 98.3(8) | N(6)−Fe(2)−N(9) | 166.2(6) |
| N(3)$^{i}$−Fe(1)−N(1) | 91.8(5) | N(7)−Fe(2)−N(8) | 164.2(6) |
| N(3)−Fe(1)−N(2)$^{i}$ | 167.0(5) | N(7)−Fe(2)−N(9) | 92.2(6) |
| N(4)−Fe(2)−N(5) | 177.6(5) | N(8)−Fe(2)−N(9) | 103.5(6) |
| N(4)−Fe(2)−N(6) | 89.6(4) | N(3)−C(9)−S(2) | 178.6(13) |
| N(4)−Fe(2)−N(7) | 88.8(4) | N(8)−C(26)−S(5) | 178(3) |
| N(4)−Fe(2)−N(8) | 88.2(5) | N(9)−C(27)−S(6) | 177(2) |
| N(4)−Fe(2)−N(9) | 92.8(5) | | |

[a] The numbers in parentheses are estimated standard deviations in the least significant digits. [b] Symmetry code: i = −*x*, −*y*, *z*.

## Results

**Structure of 1 and 2.** The crystal structures of **1**[12,24] and **2**[12] have previously been reported. Let us briefly discuss the main features of these compounds. Compounds **1** and **2** crystallize in the triclinic (P-1) and monoclinic (*I*2/*a*) space groups, respectively. Despite this fact, **1** and **2** display very similar structural motifs as they are made up of linear chains running in parallel directions. These chains consist of [Fe-$(H_2O)_2(X)_2$] (X = S, Se) planar units bridged by 4,4′-bipy ligands. Both compounds have a similar coordination environment (Figure 1a). The iron atom lies at the center of an elongated $[FeN_4O_2]$ octahedral core. The average Fe−N(4,4′-bipy) bond lengths are longer [2.212(6) and 2.214(8) Å for **1** and **2**, respectively] than those of Fe−NCX [2.133(7) Å (**1**), 2.125(6) Å (**2**)] and Fe−$OH_2$ [2.139(5) Å (**1**) and 2.101-(6) Å (**2**)]. The $NCX^-$ groups are almost linear (178°−180°) and slightly bent with respect to the Fe−N(CX) bond direction (167°−171°). The average value of the trigonal distortion angle was found to be $\Phi$ = 11° ($\Phi$ = 0° for a regular octahedron) for the two compounds, indicating a similar distortion. The pyridine rings are almost coplanar in **1** but form a dihedral angle of 16° in **2**.

A second type of 4,4′-bipy ligand intercalated between the chains is hydrogen-bonded defining a second system of zigzag chains perpendicular to the linear system of chains. The distance between the nitrogen atoms of the uncoordinated ligand and the oxygen atoms of the coordinated water molecules [O(1)····N(4)] is 2.721(9) Å (**1**) and 2.706(10) Å (**2**). Hence, uncoordinated ligands connect adjacent linear

(21) Sheldrick, G. M. *SHELXS-86, Program for Structure Determination*; University of Göttingen: Göttingen, Germany, 1990.
(22) Sheldrick, G. M. *SHELXL93 Program for the refinement of Crystal Structures*; University of Göttingen: Göttingen, Germany, 1993.
(23) Varret, F. *Proceedings of the International Conference on Mössbauer Effect Applications*, Jaipur, India, 1981; Indian National Science Academy: New Delhi, 1982.
(24) Noro, S.; Kondo, M.; Ishii, T.; Kitagawa, S.; Matsuzaka, H. *J. Chem. Soc., Dalton Trans.* **1999**, 1569.

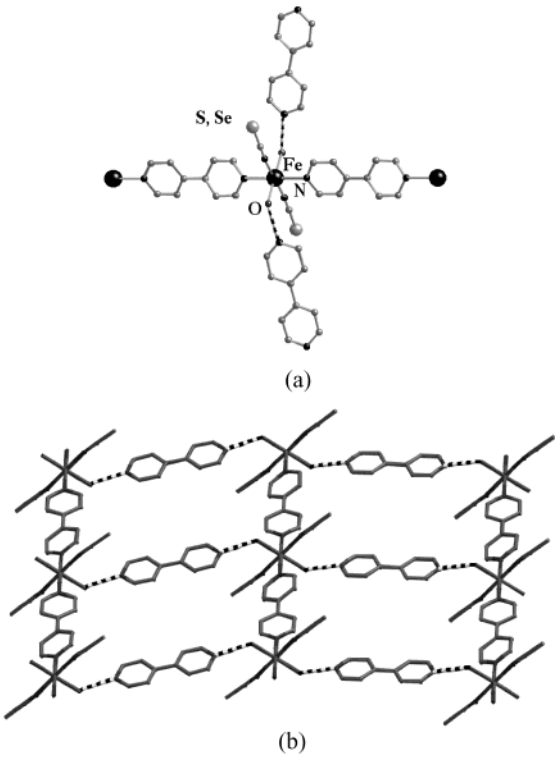


**Figure 1.** (a) Perspective view of complexes **1** and **2**. (b) Perspective view of the two-dimensional layers (dotted lines represent hydrogen bonds).

chains defining corrugated layers (Figure 1b). The layers alternate in such a way that the iron atom in an adjacent layer is above and below the center of the rectangles defined by the two systems of chains. Iron-to-iron distances through coordinated and uncoordinated 4,4′-bipy ligands are 11.41(1) and 15.51(1) Å for **1** and 11.52(1) and 15.46(1) Å for **2**, respectively.

**Structure of 3.** Compounds **3** and **4** crystallize in the orthorhombic (*Fdd*2) space group. Because of the poor quality of the single crystals of **4** the structural analysis has been only accomplished for **3**. Relevant data concerning metal-to-ligand bond distances and angles are displayed in Table 2. The molecular structure of **3** is displayed in Figure 2a together with atom numbering. Compound **3** consists of parallel linear chains running along the *y*-axis. The chains are defined by *trans*-4,4′-bipy linked iron(II) ions. The equatorial coordination plane is occupied by two nitrogen atoms of one bt ligand and two isothiocyanate groups in *cis* position.

There are two crystallographically independent chains associated with two slightly different [$FeN_6$] coordination cores (Figure 2a). The coordination octahedra are strongly distorted. The average Fe−N(4,4′-bipy), Fe−N(bt), and Fe−N(CS) bond distances are 2.222(10), 2.229(13), and 2.064(13) Å for Fe(1) and 2.252(10), 2.206(13), and 2.070(10) Å for Fe(2), respectively. The $NCS^-$ groups are linear (178°(2)) whereas the Fe−NC linkages are strongly bent [Fe(1)−N(3)−C(9) = 147.9(14)°, Fe(2)−N(8)−C(26) = 152(2)°, and Fe(2)−N(9)−C(27) = 161.0(13)°].

The 4,4′-bipy ligand strongly deviates from planarity in both type of chains, named Fe(1) and Fe(2) chains (Figure 2b). The dihedral angles between pyridine groups are 43.1(5)° and 49.5(7)° for Fe(1) and Fe(2) chains, respectively. Partial stacking of the bt ligands takes place between pairs of Fe(2) chains. The S···$S^i$ intermolecular distances between two consecutive bt ligands are 3.98 and 4.09 Å for S(3) and S(4), respectively. Iron-to-iron distance through the 4,4′-bipy ligand is 11.545(10) Å for both Fe1 and Fe2 chains. The bond angles and bond lengths within each thiazoline group compare well with those observed for the two polymorphs (A and B) of [$Fe(bt)_2(NCS)_2$].[25] Polymorph A, which is a spin-crossover system, shows slightly shorter Fe−N(bt) bonds and N−C, C−S, and C−C bond lengths on average in the bt rings than polymorph B, which is HS. Interestingly, the bt ligands in the two asymmetric units of compound **3** show very similar differences: Fe(2) chains show shorter Fe−N bond distances than Fe(1) chains; hence, C−C, C−N, and C−S bond distances are slightly shorter in Fe(2) chains.

**Magnetic Properties.** The magnetic properties of complexes **1**−**4** expressed in the form of $\chi_M T$ versus $T$ curves, where $\chi_M$ stands for the molar magnetic susceptibility and $T$ stands for the temperature, are shown in Figure 3. At room temperature, the $\chi_M T$ product is 3.46 and 3.43 $cm^3\ K\ mol^{-1}$ for **1** and **2**, respectively. These values correspond to what is expected for an iron(II) ion in the HS state and remain almost constant up to ca. 20 K, and then $\chi_M T$ drops abruptly down to 2.80 (**1**) and 3.02 (**2**) $cm^3\ K\ mol^{-1}$ at 4 K. This small decrease at very low temperatures may be understood as arising from the combined effect of spin−orbit coupling and axial distortion of the iron atom.

Compounds **3** and **4** behave quite differently from **1** and **2**. At room temperature, the $\chi_M T$ product is 3.34 and 3.36 $cm^3\ K\ mol^{-1}$ for **3** and **4**, respectively. The value of $\chi_M T$ remains almost constant when cooling to around 150 K and then diminishes rapidly to reach a value ca. 3.05 $cm^3\ K\ mol^{-1}$ at 60 K for **3**. Between 60 and 50 K, $\chi_M T$ remains almost constant at 3.05 $cm^3\ K\ mol^{-1}$ (**3**) and 2.94 (**4**) $cm^3\ K\ mol^{-1}$. Finally, $\chi_M T$ diminishes rapidly down to 1.2 $cm^3\ K\ mol^{-1}$ at 2 K for the two compounds. The first $\chi_M T$ drop is consistent with around 15% of HS ions undergoing $S = 2 \leftrightarrow S = 0$ spin-conversion (see Mössbauer Spectroscopy subsection). The second $\chi_M T$ drop can be ascribed to zero-field splitting in the orbital singlet $S = 2$ ground state arising from the strongly distorted coordination sphere of the remaining HS iron(II) ions in **3**. Compound **4** behaves essentially in a similar way as **3**; however, the $\chi_M T$ drop due to the spin-conversion starts at higher temperatures as is usually observed for $NCSe^-$ compared to $NCS^-$.

**Mössbauer Spectroscopy.** Representative Mössbauer spectra of **3** and **4** are shown in Figure 4. The prominent high-temperature doublet (230 K) and the weak low-temperature doublet (80 K) of complex **3** are typical of iron(II) in the HS and LS states, respectively. The isomer shifts, $IS_{HS} = 1.020(1)$ mm $s^{-1}$ and $IS_{LS} = 0.458(7)$ mm $s^{-1}$, and quadrupole splitting values, $\Delta E_Q(HS) = 2.715(3)$ and $\Delta E_Q(LS) = 0.80(1)$ mm $s^{-1}$, are in agreement with those previously published for iron(II) spin-crossover compounds.

(25) Ozarowski, A.; McGarvey, B. R.; Sarkar, A. B.; Drake, J. E. *Inorg. Chem.* **1988**, *27*, 628.

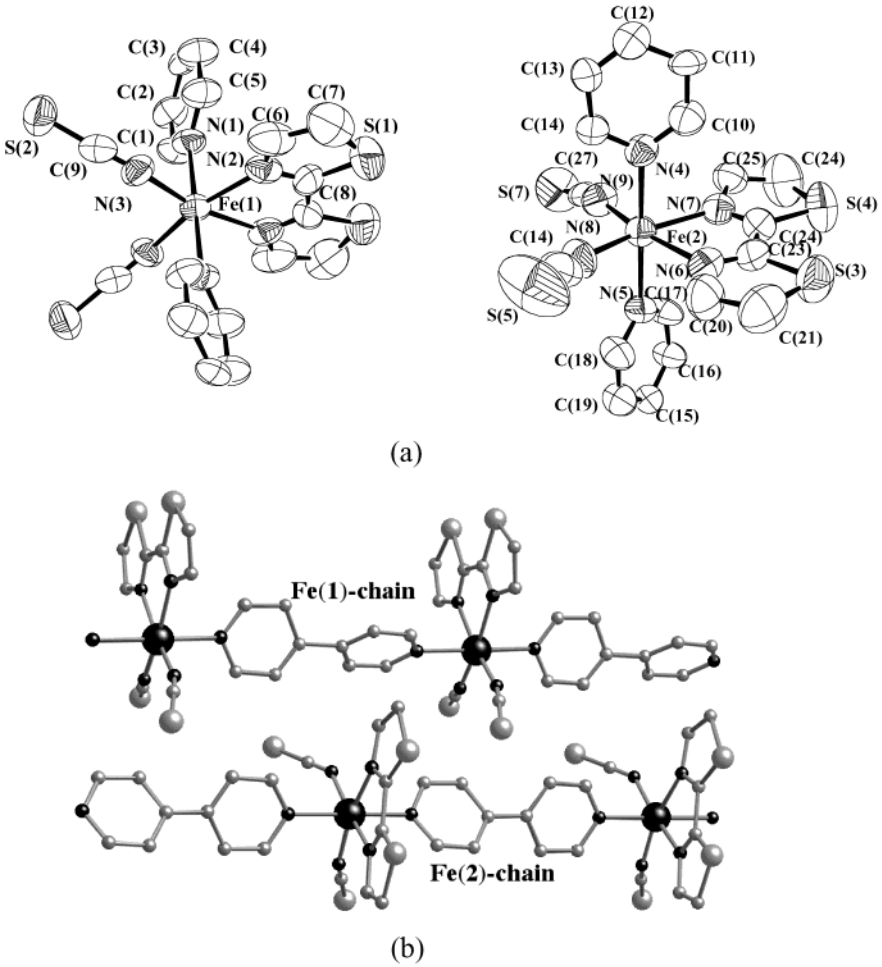


**Figure 2.** (a) View of the Fe(1) (left) and Fe(2) (right) sites in **3** (thermal vibrational ellipsoids are at 40% probability level, and H atoms have been omitted for clarity). (b) Perspective view showing the relative disposition of two consecutive Fe(1) and Fe(2) chains of **3**.

Detailed values of the Mössbauer parameters resulting from the least-squares fitting procedures are listed in Table 3. The thermal variation of $\Delta E_Q$(HS) is shown in Figure 5. The large $\Delta E_Q$(HS) values (2.715(3)−3.001(1) mm s$^{-1}$) between 230 and 4.5 K indicate a local symmetry lower than cubic with a rather well-isolated ground orbital singlet. The small $\Delta E_Q$(HS) variation in this temperature range is characteristic of a strongly distorted octahedral environment. It is possible to roughly access the average energy $\delta$ of the excited orbital states belonging to the cubic triplet (inset in Figure 5) assuming that the $\Delta E_Q$(HS) slope varies as $\delta^{-1}$.[26] The slope $d\Delta E_Q(HS)/dT$ can be accurately determined as $-1.80 \times 10^{-3}$ mm s$^{-1}$ K$^{-1}$ yielding a $\delta$ value of 918 cm$^{-1}$. A similar behavior was reported for HS iron(II) ions in $K_2ZnF_4$ matrix, with a slope of $-2.82 \times 10^{-3}$ mm s$^{-1}$ K$^{-1}$.[27] The data were analyzed in a full vibronic treatment and led to $\delta = 590$ cm$^{-1}$. Concerning complex **4**, the prominent high-temperature doublet (293 K) and the weak low-temperature doublet (80 K) are typical of iron(II) in the HS and LS states, respectively. The isomer shifts, $IS_{HS} = 1.096(2)$ mm s$^{-1}$ and $IS_{LS} = 0.38(2)$ mm s$^{-1}$, and quadrupole splitting values, $\Delta E_Q$(HS) = 2.742(5) and $\Delta E_Q$(LS) = 0.44(2) mm s$^{-1}$, are in agreement with those previously published for iron(II) spin-crossover compounds. Detailed values of the Mössbauer parameters resulting from least-squares fitting procedures are listed in Table 4. Moreover, we can observe a second high-spin doublet (a: IS = 1.10(1) mm s$^{-1}$ and $\Delta E_Q$(HS) = 3.15(1) mm s$^{-1}$ at 293 K) corresponding to an impurity. The fitting of the Mössbauer spectra showed the presence of 12.62% of the precursor compound **2** (see Supporting Information). This impurity is found as very small red microcrystals, which can be separated by hand using a binocular lens when the required amount of sample is small. However, because of the strong absorption of the Se atom, an amount of at least 100 mg is required to obtain clean Mössbauer spectra in a reasonable time length, and consequently, it was not affordable to carry out the Mössbauer measurements with a pure sample of **4**. The resulting thermal variations of the high-spin molar fraction, $n_{HS}$ (relative area ratio), for **3** and **4** are shown in Figure 6 (● (**3**) and ▲ (**4**)). The low-spin state for both complexes can be detected at all temperatures: they smoothly vary from ∼12% (**3**) and ∼21% (**4**) at 4.5 K to ∼3% at 230 K for **3** and at 293 K for **4**. The obtained data are in good agreement with the smooth thermalvariation of $\chi_M T$ in the high-temperature range for both complexes.

(26) Real, J. A.; Bolvin, H.; Bousseksou, A.; Dworkin, A.; Kahn, O.; Varret, F.; Zarembowitch, J. *J. Am. Chem Soc.* **1992**, *114*, 4650.
(27) Ducouret-Cérese, A.; Varret, F. *J. Phys. (Paris)* **1988**, *49*, 661.

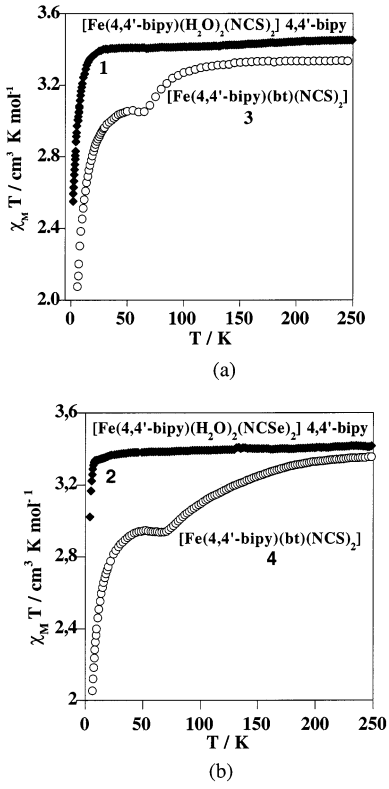


**Figure 3.** Thermal variation of the $\chi_M T$ product for **1** and **3** (a) and for **2** and **4** (b).

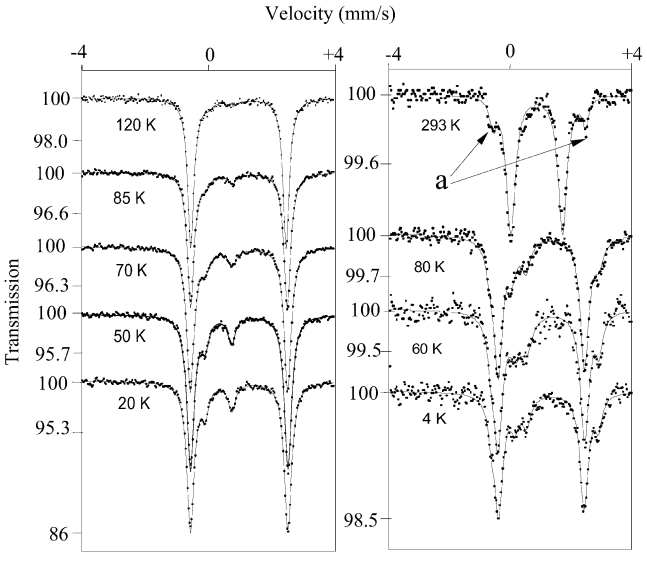


**Figure 4.** Selected Mössbauer spectra for **3** (left) and for **4** (right) obtained in the cooling mode between room temperature and 4.5 K. The solid lines (—) represent fitted curves. The doublet (a) represents the spectrum of the precursor complex, **2** (≈12% impurity) (see text).

## Discussion

We would like to emphasize two main aspects of the present work: on one hand, the search for rational strategies to synthesize new polymeric spin-crossover compounds and, on the other hand, the nature of the very incomplete spin-conversion observed for **3** and **4**. Concerning the former aspect, it is well-known that ligands such as 1,2-di-(4-pyridyl)-ethylene (bpe), 1,4-bis-(4-pyridyl)-butadyine (bpb), and 4,4′-bis-1,2,4-triazole (btr) represent good examples of rodlike bifunctional ligands well-suited for the synthesis of spin-crossover coordination polymers.[6,8,11] Upon reaction of these ligands with [iron(II)/2NCX$^-$] solutions, the solvent molecules of the first coordination sphere of the metal ion are usually replaced yielding square-grid motifs as observed in the [Fe(btr)$_2$(NCX)$_2$]·H$_2$O (X = S, Se),[6,7] [Fe(bpe)$_2$(NCS)$_2$]·CH$_3$OH,[8] and [Fe(bpb)$_2$(NCS)$_2$]·0.5CH$_3$OH[11] spin-crossover systems. Further, the synthesis of the [Fe(btr)$_3$(ClO$_4$)$_2$]$_n$ 3D polymeric spin-crossover compound through substitution of pseudohalide anions with noncoordinating anions such as ClO$_4^-$ has been recently reported.[10] Extrapolation of these results to the 4,4′-bipy ligand is not valid because of the formation of very effective hydrogen bonds between the uncoordinated organic ligand (L) and the coordinated solvent molecules. It is apparent that this fact prevents further substitution of solvent molecules by L because of the formation of very stable [Fe(L)(solvent)$_2$(NCX)$_2$]·L linear chains. Recently, the crystal structure of [Co(4,4′-bipy)$_2$(NCS)$_2$]·2(CH$_3$CH$_2$)$_2$O has been reported. Single crystals of this compound were obtained from slow diffusion of two solutions, one containing 4,4′-bipy in ethyl ether and the other one containing [Co(NCS)$_2$] in methanol.[16] Our attempts to synthesize a similar compound with iron(II) were unsuccessful.

**Table 3.** Representative Least-Squares-Fitted Mössbauer Data for **3**[a]

| | low-spin state | | | high spin-state | | | $A_{HS}/A_{tot}$ |
|---|---|---|---|---|---|---|---|
| $T$ (K) | IS | $\Delta E_Q$(LS) | Γ/2 | IS | $\Delta E_Q$(HS) | Γ/2 | (%) |
| 230 | 0.47(1) | 0.65(4) | 0.24(1) | 1.020(1) | 2.715(3) | 0.144(2) | 96.5(4) |
| 200 | 0.48(2) | 0.67(5) | 0.18(1) | 1.03(1) | 2.788(2) | 0.131(2) | 95.6(5) |
| 120 | 0.49(2) | 0.71(5) | 0.18(3) | 1.069(1) | 2.935(2) | 0.117(1) | 93.9(7) |
| 90 | 0.46(2) | 0.78(3) | 0.14(2) | 1.079(1) | 2.968(2) | 0.121(1) | 92.7(5) |
| 85 | 0.464(9) | 0.81(1) | 0.14(1) | 1.086(1) | 2.973(1) | 0.126(1) | 91.9(5) |
| 80 | 0.458(7) | 0.80(1) | 0.14(1) | 1.083(1) | 2.979(1) | 0.121(1) | 91.5(4) |
| 70 | 0.466(6) | 0.80(1) | 0.145(8) | 1.085(1) | 2.991(1) | 0.136(1) | 87.9(4) |
| 65 | 0.439(5) | 0.81(1) | 0.156(7) | 1.086(1) | 2.996(1) | 0.135(1) | 85.0(4) |
| 60 | 0.444(4) | 0.828(8) | 0.149(6) | 1.088(1) | 2.997(1) | 0.133(1) | 85.0(3) |
| 55 | 0.456(5) | 0.832(9) | 0.142(6) | 1.089(1) | 3.005(1) | 0.136(1) | 85.,3(4) |
| 50 | 0.448(4) | 0.812(7) | 0.132(5) | 1.091(1) | 3.001(1) | 0.134(1) | 85.1(4) |
| 35 | 0.448(4) | 0.812(8) | 0.140(5) | 1.092(1) | 3.002(1) | 0.136(1) | 84.5(3) |
| 20 | 0.451(4) | 0.819(7) | 0.132(5) | 1.092(1) | 2.998(1) | 0.136(1) | 84.8(4) |
| 4 | 0.437(6) | 0.835(9) | 0.132(8) | 1.094(1) | 3.001(1) | 0.142(1) | 86.5(5) |

[a] Isomer shift (IS) refers to metallic iron at room temperature (1 mm s$^{-1}$ = 1.12 × 107 s$^{-1}$), $\Delta E_Q$ = quadrupole splitting (mm s$^{-1}$), Γ/2 = half-width of the lines (mm s$^{-1}$), and statistical standard deviations are given in parentheses.

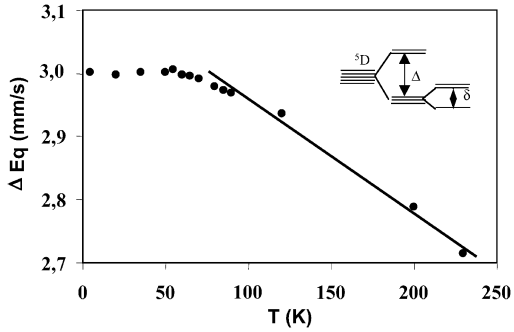


**Figure 5.** Thermal variation of the quadrupole splitting of the high-spin doublet obtained from the Mössbauer measurements of **3** carried out in the cooling mode. The insert depicts the ligand-field splitting of the high-spin state. The full line represents a linear regression leading to a slope of −1.80 × 10$^{-3}$ mm s$^{-1}$ K$^{-1}$.

**Table 4.** Representative Least-Squares-Fitted Mössbauer Data for **4**[a]

| | low-spin state | | | high-spin state | | | impurity | | | $A_{HStot}/A_{tot}$ |
|---|---|---|---|---|---|---|---|---|---|---|
| $T$ (K) | IS | $\Delta E_Q$(LS) | $\Gamma/2$ | IS | $\Delta E_Q$(HS) | $\Gamma/2$ | IS | $\Delta E_Q$(HS) | $\Gamma/2$ | (%) |
| 293 | | | | 1.007(3) | 1.761(6) | 0.182(5) | 1.10(1) | 3.15(3) | 0.13(2) | 100(2) |
| 80 | 0.38(2) | 0.44(2) | 0.17(2) | 1.096(2) | 2.742(5) | 0.166(4) | 1.21(2) | 3.40(3) | 0.16(4) | 83(2) |
| 60 | 0.38(3) | 0.45(3) | 0.22(5) | 1.098(4) | 2.760(8) | 0.168(3) | 1.21(2) | 3.41(3) | 0.14(2) | 77(2) |
| 4.5 | 0.38(3) | 0.44(2) | 0.17(3) | 1.103(3) | 2.784(7) | 0.155(6) | 1.22(1) | 3.43(2) | 0.12(2) | 79(3) |

[a] Isomer shift (IS) refers to metallic iron at room temperature (1 mm $s^{-1}$ = 1.12 × 107 $s^{-1}$), $\Delta E_Q$ = quadrupole splitting (mm $s^{-1}$); $\Gamma/2$ = half-width of the lines (mm $s^{-1}$), and statistical standard deviations are given in parentheses.

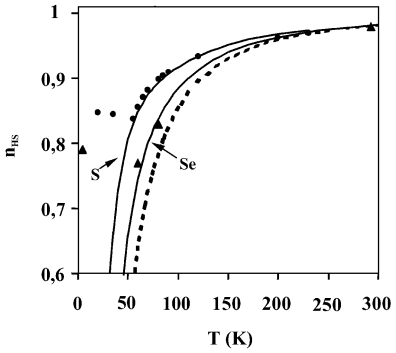


**Figure 6.** Thermal variation of the high-spin molar fraction, $n_{HS}$, deduced from Mössbauer spectroscopy: [Fe(4,4′-bipy)(bt)$(NCS)_2$] (**3**) (●); [Fe(4,4′-bipy)(bt)$(NCSe)_2$] (**4**) (▲). Solid lines (—) correspond to the fit obtained by using the electrovibrational model (see text). The dashed line (- - -) is the $n_{HS}(T)$ curve calculated with the $\Delta$ and $\omega_{LS}/\omega_{HS}$ parameters obtained for complex **3** ($NCS^-$) and a theoretical $\omega_{LS(4)}$ value such that $\omega_{LS(3)}/\omega_{LS(4)}$ is in the 1.09 (Se/S) molar mass ratio.

As illustrated here, solubility in water/methanol makes these undesirable species suitable starting materials for the synthesis of new 1D spin-crossover compounds by choosing convenient imine ligands capable of replacing the coordinated solvent molecules.

Concerning the spin-conversion observed in **3** and **4**, it is worth noting that a similar spin-conversion has been already studied in the case of $[Fe(TRIM)_2]F_2$, where TRIM is 4-(4-imidazolylmethyl)-2-(2-imidazolylmethyl)-imidazole,[18a] and [$Fe^{II}$(3-MeO,5-$NO_2$-sal-N(1,10)-Nme(4,7))].[18b] The magnetic behavior of **3** and **4** is similar and suggests that the HS and LS states are nearly degenerated. In this case, the temperature characteristic of the spin-transition, $T_{1/2}$, at which $n_{HS} = 0.5$, is low to the point that a very incomplete spin-conversion is observed because of thermal quenching. This partial spin-conversion in Fe(II) spin-crossover compounds with $T_{1/2} <$ 120 K results from slow kinetics.[3] In the present case, the quenching effect is observed at $T_Q <$ 64 and 72 K for **3** and **4**, respectively.

For nearly degenerated systems, the spin-conversion is no longer governed by the electronic gap-energy but by the progressive population of the vibrational levels associated with the HS and LS states. Then, the variation of the HS molar fraction, $n_{HS}$, cannot be interpreted with macroscopic thermodynamic models such as that of Slichter and Drickamer,[28] or their Ising-type (i.e., two-level) microscopic equivalents.[29] Hence, a vibrational extension as developed with the macroscopic thermodynamic approach,[30] or its Ising-like counterpart,[19] is required. Following the simplified approach based on the Ising-type model, completed with harmonic oscillators associated with the 15 vibrational modes of the coordination octahedron, the partition function associated with the electrovibrational Hamiltonian neglecting cooperative interactions is written in the following adiabatic (and harmonic) approximation:[18a,19]

$$ZZ(T) = g_{LSe}ZZ_{vib}^{LS}(T) + g_{HSe}ZZ_{vib}^{HS}(T)e^{-\Delta(n_{HS})/k_BT} \quad (1)$$

where $\Delta(n_{HS})$ is the energy gap between the high-spin and low-spin states depending on the cooperative interactions of the system. In the frame of the Ising-like model,[19a,18] $\Delta = \Delta_0 - 4Jn_{HS}$, $\Delta_0$ is the electronic energy gap between HS and LS states of the molecule, and $J$ is the average of cooperative interactions in the system. The electronic degeneracies of the two states, $g_{LSe}$ and $g_{HSe}$, take the spin-only values (5 and 1 for HS and LS states, respectively) because the orbital degeneracy of the $^5T_{2g}$ state is lifted by the low-symmetry components of the ligand field, as evidenced by the large value of the quadrupole splitting in the Mössbauer spectra. For each state, the vibrational function partition is written as follows:

$$ZZvib(T) = \prod_{i=1}^{p} Zvib(\omega_i, T) \quad (2)$$

where $\omega_i$ is the frequency of the $i$th vibration mode, characterized by different values in the LS and HS states. $Z$vib($\omega_i$, $T$) is the partition function of the isolated harmonic $i$th oscillator (in the LS or HS state).

For simplicity, we have averaged the 15 vibrational modes of the [$FeN_6$] core, assuming a single frequency for each spin-state ($\omega_{LS}$ and $\omega_{HS}$ for the LS and HS states, respectively). By thermal averaging, the equilibrium constant of the system ($K_{eq} = n_{HS}/n_{LS}$) is obtained for each temperature, leading to $n_{HS}(T)$ as function of temperature through numerical resolution of the following self-consistent equation:

$$K_{eq}(T) = \frac{n_{HS}}{n_{LS}} = \frac{g_{HSe}ZZ_{vib}^{HS}(T)}{g_{LSe}ZZ_{vib}^{LS}(T)}e^{-\Delta/k_B \cdot T} \quad (3)$$

(28) (a) Slichter, C. P.; Drickamer, H. G. *J. Chem. Phys.* **1972**, *56*, 2142. (b) Purcell, K. F.; Edwards, M. P. *Inorg. Chem.* **1984**, *23*, 2620.

(29) (a) Bari, R. A.; Sivardière, J. *Phys. Rev. B* **1972**, 4466. (b) Wajnflasz, J. *J. Phys. C* **1970**, *40*, 537. (c) Bousseksou, A.; Nasser, J.; Boukheddaden, K.; Varret, F. *J. Phys. I* **1992**, *2*, 1381. (d) Bousseksou, A.; Nasser, J.; Boukheddaden, K.; Varret, F. *Mol. Cryst Liq. Cryst.* **1993**, *234*, 269.

(30) Spiering, H.; Maissner, E.; Köppen, H.; Müller, E. W.; Gütlich, P. *Chem Phys.* **1982**, *68*, 65.

It is significant to recall that this model predicts the existence of a critical situation as forecasted in refs 19 and 31. Indeed, when the electronic energy gap $\Delta$ between the HS and LS states of the molecule is of the same order of magnitude as the vibrational contribution $(15/2)\hbar(\omega_{LS} - \omega_{HS})$, the ground state of the system may be the HS state. In this critical situation, one can observe a HS $\rightarrow$ LS $\rightarrow$ HS conversion as shown in Figure 6 of ref 19. Of course, the HS $\rightarrow$ LS conversion is not complete: the system remains mainly in the HS state, and one observes approximately 5−20% of molecules in the LS state.

As established in ref 19b−d, working assumptions are needed to interpret correctly the whole vibrational contributions to the thermal variation of $n_{HS}(T)$. Raman spectroscopy of both complexes is in progress. In the present work, for simplicity, only averages of the 15 octahedron vibrational modes in the HS and LS states are considered. The least-squares fitting of the high-temperature range of the $n_{HS}$ versus $T$ curve ($T > T_Q$) leads to an excellent agreement with the experimental data, as shown by the solid line in Figure 6. The values of the fitted parameters are $\Delta = 597$ cm$^{-1}$, $\omega_{LS} = 382$ cm$^{-1}$, and $\omega_{LS}/\omega_{HS} = 1.22$ for **3**. These parameters enable us to estimate the electrovibrational energy gap between the fundamental (LS) and the first excited state (HS) ($\Delta_{eff} = \Delta - (15/2)\hbar(\bar{\omega}_{LS} - \bar{\omega}_{HS})$ to ~65 cm$^{-1}$. With such a small energy difference, the lowest LS and HS states are almost equienergetic, and the thermal dependence of the system only occurs through population of vibrational states.

**Mass Effect.** Upon substitution of hydrogen with deuterium in methanol and ethanol solvates[32] of $[Fe(2\text{-pic})_3]Cl_2$ and $Fe^{II}(5\text{-}NO_2\text{-Sal-}N(1,4,7,10))$],[33] an isotopic effect on the transition temperature ($T_{1/2}$) was observed: the spin-crossover curve $n_{HS}(T)$ is shifted toward high temperatures in the deuterated complexes as a consequence of higher $T_{1/2}$ values. This effect was interpreted as the consequence of the lowering in intramolecular vibration frequencies that resulted from the mass effect associated with the substitution of hydrogen with deuterium.[19,29b,32−34] In agreement with the observed isotopic effect, the plot of $T_{1/2}$ as a function of the average intramolecular vibration frequency ($\bar{\omega}$) shows that $T_{1/2}$ decreases when $\bar{\omega}$ increases.[29d,34]

As shown in Figure 7, the decrease in average frequency of intramolecular vibrations ($\bar{\omega}$) corresponding to an equienergetic situation also shifts the conversion curve toward high temperatures, even though the $n_{HS}$ variation is small in such equienergetic situations.

An identical effect, i.e., lowering of the average frequency of intramolecular vibrations, may be expected upon substitution of any atom with a heavier one in the complex molecule provided a mass effect on Fe−L bonds may result from the substitution. With this purpose, we substituted the coordinated $NCS^-$ anions of complex **3** with $NCSe^-$ anions (complex **4**). As shown in Figure 6, the $n_{HS}$ versus $T$ data obtained for complex **4** ($NCSe^-$, ▲) compared to those for complex **3** ($NCS^-$, ●) clearly indicate that a significant shift in $T_{1/2}$ results from this mass effect.

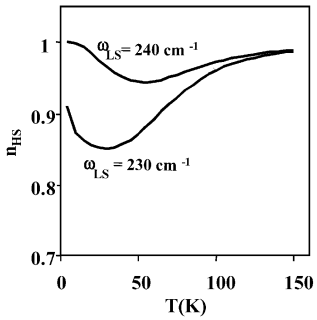


**Figure 7.** Set of theoretical $n_{HS}(T)$ curves in the equienergetic states situation ($\Delta_{eff} \sim 0$) and for (a) $\omega_{LS} = 240$ cm$^{-1}$, (b) $\omega_{LS} = 230$ cm$^{-1}$.

To estimate this mass effect on the average frequency of intramolecular vibrations ($\bar{\omega}$), the electronic parameter $\Delta$ and the ratio $\omega_{LS}/\omega_{HS}$ were set to the values obtained for complex **3** ($NCS^-$, $\Delta = 597$ cm$^{-1}$, $\omega_{LS}/\omega_{HS} = 1.22$) during the fitting procedure for complex **4** ($NCSe^-$). The least-squares fit of the $n_{HS}$ versus $T$ data of complex **4** (high-temperature range, $T > T_Q$) leads to an excellent agreement with the experimental data, as shown in Figure 6 ($NCSe^-$ solid line). The 365 cm$^{-1}$ $\omega_{LS(4)}$ value resulting from the fit carried out for **4** ($NCSe^-$) is significantly lower than the 382 cm$^{-1}$ $\omega_{LS(3)}$ value resulting from the fit carried out for **3** ($NCS^-$). The ca. 1.05 $\omega_{LS(3)}/\omega_{LS(4)}$ ratio is close to the ca. 1.09 $\bar{\omega}_{Se}/\bar{\omega}_S$ estimated from the classical formula:

$$\bar{\omega}_{i,j} = \frac{1}{2\pi}\sqrt{\frac{f_i}{M_j}} \quad i = \text{HS, LS; } j = \text{S, Se}$$

where the force constants, $f_i$, are considered identical for **3** and **4** and $M_j$ is the corresponding molar mass. The best fit parameters obtained for complex **4** also enable us to estimate the electrovibrational energy gap between the ground state (LS) and the first excited state (HS): $\Delta_{eff} \approx 86$ cm$^{-1}$.

It is also interesting to compare the experimental $n_{HS}$ versus $T$ data of complex **4** ($NCSe^-$) to the theoretical $n_{HS}(T)$ curve calculated with the $\Delta$ and $\omega_{LS}/\omega_{HS}$ parameters obtained for complex **3** ($NCS^-$) and a theoretical $\omega_{LS(4)}$ value such that $\omega_{LS(3)}/\omega_{LS(4)}$ is in the 1.09 (Se/S) molar mass ratio. The dashed line in Figure 6 showing the corresponding theoretical curve is close to the experimental $n_{HS}$ versus $T$ data of complex **4** ($NCSe^-$). As a whole, these results confirm that the observed effect, obtained for the first time in an equienergetic spin-crossover complex, is clearly a mass effect.

An important question remains, however: Which modes are most affected, the bending or the stretching modes? This question will be addressed through future investigations with Raman and/or infrared spectroscopy.

(31) Zimmerman, R.; König, E. *J. Phys. Chem. Solids* **1977**, *38*, 779.
(32) Gütlich, P.; Köppen, H.; Steinhäuser, G. *Chem. Phys. Lett.* **1980**, *74*, 475.
(33) Bousseksou, A.; Tommasi, L.; Lemercier, G.; Varret, F.; Tuchagues, J.-P. *Chem. Phys. Lett.* **1995**, *243*, 493.
(34) Bousseksou, A. Ph.D. Thesis, Université Pierre et Marie Curie, Paris 6, 1992.

**Acknowledgment.** We thank the financial assistance from the Ministerio Español de Ciencia y Tecnología (Project BQU 2001-2928). We acknowledge the European Commission for granting the TMR-Network "Thermal and Optical Switching of Molecular Spin States (TOSS)", Contract nº-ERB-FMRX-CT98-0199EEC/TMR.

**Supporting Information Available:** Figure S1, giving the compared Mössbauer spectra of **2** and the impure sample of **4**. X-ray crystallographic file for **3**, in CIF format. This material is available free of charge via Internet at http://pubs.acs.org.

IC0203825